Article

Cobalt Oxide on a Nanoporous TUD-1 Catalyst for Methylene Blue Dye Interaction DFT Studies and Degradation

Muthusamy Poomalai Pachamuthu [1,*], Sambath Baskaran [2,*], Chandrakumar Manivannan [1], Somasundaram Chandra Kishore [3,*], Stefano Bellucci [4] and Ramasamy Boopathy [5]

1   Department of Chemistry, Sensors Lab, Bannari Amman Institute of Technology, Sathyamangalam 638401, India; cmanivannan89@gmail.com
2   Department of Chemistry, Southern University of Science and Technology, Shenzhen 518055, China
3   Department of Biomedical Engineering, Saveetha Institute of Medical and Technical Sciences (SIMTS), Saveetha School of Engineering, Saveetha University, Chennai 602105, India
4   INFN-Laboratori Nazionali di Frascati, 00044 Frascati, Italy; stefano.bellucci@lnf.infn.it
5   Environment & Sustainability Department, CSIR-Institute of Minerals and Materials Technology, Bhubaneswar 751013, India; boopathy@immt.res.in
*   Correspondence: pachachem@gmail.com (M.P.P.); baskarsambath@gmail.com (S.B.); schandrakishore30@gmail.com (S.C.K.)

Abstract: Fenton and Fenton-like advanced oxidation processes (AOP) have been substantially utilized in wastewater treatment for the removal of organic contaminants. The present investigation explores the catalytic activity of cobalt dispersed over nanoporous silicate material (CoO/TUD-1), TUD-1, for the Fenton-type degradation of methylene blue (MB) dye present in wastewater, with hydrogen peroxide (H_2O_2) as an oxidant. The catalyst, which was prepared using the hydrothermal method, was characterized using analytical and spectroscopic techniques, such as X-ray diffraction (XRD), N_2 adsorption–desorption isotherms, UV-visible diffuse reflectance (DR), scanning electron microscope (SEM), transmission electron microscopy (TEM) and Fourier transform infrared (FTIR). The results indicated that the CoO/TUD-1 possessed three-dimensional structures with a high surface area and a pore diameter capable of the uniform dispersion of cobalt species. Density functional theory (DFT) simulations were performed to study the most stable tetra coordinate adsorption configuration of a single Co atom on amorphous SiO_2. To understand the geometric and electronic structure of this configuration, electron density differences, Bader charge, and partial density of states were examined. The results obtained from the DFT calculations confirmed the occurrence of electron transfer from the Co atom to the amorphous SiO_2. The calculated adsorption energy was found to be -1.58 eV, which indicated that the MB dye was strongly adsorbed by parallel configuration mode and degraded more easily. Further, the addition of a 0.1g/L dose of the prepared CoO /TUD degraded the MB dye effectively (~95%) within 240 min of contact. Thus, CoO/TUD-1 is a potential material for the removal of organic contaminants and the degradation of dyes in wastewater treatment.

Keywords: mesoporous; TUD-1; methyl blue degradation; density functional theory

1. Introduction

Over the past decade, water treatment and purification have been a significant are of concern in the fields of chemical and environmental science [1–3]. With the rapid growth of the textile and dye industries, more and more essential commercial dyes and several other synthetic toxic chemicals are dumped through various means into water bodies. Methylene blue (MB), a heterocyclic aromatic chemical compound with the molecular formula $C_{16}H_{18}ClN_3S$ is one of the most commonly used thiazine dyes in the textile, paper, fabrics, food and cosmetics industries [4,5]. This dye is anti-biodegradable and incompatible with bases, reducing and strong oxidizing agents. In case of a chemical reaction, this dye compound completely removes the dissolved oxygen present in water bodies and also

discharges various toxic compounds that are hazardous to ecosystems [5]. In humans and animals it can cause severe damage to eyes, unpleasant respiration after inhalation, nausea, diarrhea, excessive sweating, mental discomfort and methemoglobinemia [6].

There are various methods available for the removal of MB, such as photocatalytic degradation [7], biological degradation [8], advanced chemical oxidation [9], nano filtration [10] and ultra-filtration [11]. Advanced oxidation processes (AOPs) are an important method for wastewater treatment [12,13]. Fenton or photo-Fenton reactions are known to be a promising class of AOP. These reactions use an iron-based catalyst that can react with H_2O_2 (oxidizing agent) to release hydroxide radicals (●OH) that result in the degradation of various organic contaminants into non-toxic by-products [14–19]. The classical homogeneous Fenton reagent comprising Fe^{2+} and H_2O_2 has been shown to be of useful degradation ability and general scope, although the need for acidic conditions to avoid the hydrolysis of ferrous and ferric ions and the removal of iron ion-containing sludge make this process costly and unsustainable. Heterogeneous methods of Fenton employing solid catalysts, such as iron oxide nanoparticles, were explored as a potential solution [20]. However, these technologies focused on nanoparticles and demonstrated with many pitfalls, such as high metal ion leaching, low catalytic performance, agglomeration of nanoparticles, and high recovery costs.

The heterogenization of the homogeneous catalysts offers a variety of advantages as it involves simplicity of isolation and reusability of the catalyst. Several heterogeneous catalysts were widely studied for cobalt-based catalytic systems, such as Co_3O_4 and $CoFeO_4$ nanoparticles, which suffered leaching problems [21,22]. Various efforts were devoted to immobilize the cobalt species on several supports, such as graphene oxide, activated carbon, carbon nanotube, titanium oxide and magnesium oxide [23–25]. Nonetheless, such catalytic supports suffered from high-cost materials synthesis, and their low catalytic activity performance, due to their lower porosity, hindered the development of various chemical reactions. In general, methylene blue (MB) is low-biodegradable in nature; it was therefore essential to have catalytic material with a high degradation capability. TUD-1 is a three-dimensional mesoporous silica material with high thermal stability and a sponge-like structure with tunable pores, which create a significantly large surface area [26–30].

Recently, we reported an efficient, simple, one-pot hydrothermal synthesis method of cobalt-incorporated amorphous disordered mesoporous silica, TUD-1 [29]. These catalysts proved to be catalytically active and better candidates compared to other ordered mesoporous materials. The presence of Co-atrane and silatrane complexes during the synthesis of TUD-1 enables a broad dispersion of Co species within or at the surface of the silica network. These materials have the benefit of incorporating higher concentrations of active metal ion species with relatively similar distributions of pore size, thus evading the leaching effect. The redox, acid base, physicochemistry, and behavior of nanostructured catalysts, and therefore their interaction with dye molecules, are all tuned by symmetry in terms of particle size and shape, yielding unique catalytic activity. The present investigation reports on the economical synthesis and characterization of cobalt-oxide-impregnated TUD-1 material suitable for the adsorption, followed by degradation, of MB. In addition, DFT studies were also carried out to study the most stable adsorption configuration of a single Co atom on amorphous SiO_2. The geometric and electronic structure of the configuration were studied based on electron density differences, Bader charge and partial density of states. The binding energy of MB at various possible configurations was also investigated. The catalytic activity of CoO/TUD-1 was studied through the degradation of MB, thus exploiting its potential application for the removal of organic pollutants.

2. Materials and Methods

2.1. Materials

Tetraethyl orthosilicate (98%, TEOS, ACROS, Carlsbad, CA, USA), triethanolamine (97%, TEA, ACROS, Carlsbad, CA, USA), tetraethyl ammonium hydroxide (35%, TEAOH,

Aldrich, St. Louis, MO, USA), cobalt nitrate ($Co(NO_3)_2 \cdot 3H_2O$, Merck, Germany) and double distilled water.

2.2. Catalyst Synthesis

As reported in our previous works, a mesoporous TUD-1 sample was prepared by aging, drying, and calcining a homogeneous synthesis mixture comprising a tetraethyl orthosilicate (TEOS) as a silicon alkoxide precursor and triethanolamine (TEA) [29]. A mixture of TEA (97%, ACROS, Carlsbad, CA, USA) and H_2O was added dropwise into TEOS (98%, ACROS, Carlsbad, CA, USA) under stirring. Lastly, tetraethyl ammonium hydroxide (TEAOH, 35%, Aldrich, St. Louis, MO, USA) was applied dropwise. A smooth and pale yellow solution was obtained after stirring for 2 h, with a molar ratio composition of $1SiO_2:0.3TEAOH:1TEA:11H_2O$. The mixture was aged for 24 h at room temperature, dried for 24 h at 373 K, hydrothermally treated for 4 h in a Teflon-lined stainless steel autoclave, and then calcined for 10 h at 873 K. 10 wt.% of cobalt oxide supported on Si-TUD-1 was prepared by the conventional impregnation method using cobalt salt solution. Finally, the obtained material was named as CoO/TUD-1.

2.3. Characterization

The X-ray diffraction (XRD) measurement was carried out on a Rigaku, Japan diffractometer with a Cu Kα (λ = 1.5418 Å) radiation source in the 2θ range 10–80°. The BET isotherm was evaluated from nitrogen sorption carried out at -196 °C using a Micromeritics ASAP 2020, USA porosimeter. The transmission electron microscopy (TEM) was performed on a FEI Tecnai G2, USA fitted with a CCD camera. The FTIR spectra of KBr-diluted pellets from the sample were recorded on a FTIR-Bruker (Tensor), Germany instrument measured in the range of 4000 to 400 cm^{-1}. The UV-visible diffuse reflectance spectra of the samples were recorded on a thermo scientific, (Evolution 600) UK spectrometer.

2.4. Computational Methods

All spin polarization calculations were conducted by density functional theory (DFT) level using the Vienna ab initio simulation package (VASP) [30–32]. The projector-augmented wave (PAW) method was used to define the interactions between the ion cores and valence electrons and the generalized gradient approximation (GGA)-Perdew−Burke−Ernzerhof (PBE) exchange−correlation function was implemented [33,34]. The plane wave kinetic energy cut off of fixed to be 450 eV. The Brillouin zone in the reciprocal space was sampled by the $1 \times 1 \times 1$ Γ point. All the ions were allowed to relax until the maximum force was less than 0.03 eV/Å. Van der Waals interactions were applied using the DFT-D3 approach, as employed in VASP [35]. The electron charge transfer was calculated using grid-based Bader analysis [36,37].

2.5. Fenton Oxidation Reaction

The Fenton oxidation of MB was carried out in a 1000 mL polypropylene bottle fitted with a magnetic stirrer. The catalytic activity of the catalyst was evaluated according to the degradation of MB (100 ppm) by the batch process under a 100 rpm stirring speed at room temperature. A total of 100 mL of methylene blue solution (100 ppm) and 6.4 mmol/L of H_2O_2 (30%) were added to the bottle. To initiate the degradation, known MB solution was mixed with the H_2O_2 oxidant and stirred. Finally, 0.1g/L of the preheated catalyst CoO/TUD-1 were added and the reaction flask was kept in the stirrer at room temperature. The samples were withdrawn periodically and analyzed using the UV-visible spectrophotometer. The conversion and product selectivity were calculated based on the peak intensity and concentration variations. The MB degradation was calculated from the following expression:

$$\text{Percentage degradation} = [C_o - C_t/Co] * 100$$

where C_o = Initial concentration of the dye solution and C_t = Concentration remaining after irradiation at time t.

3. Results and Discussion

3.1. Characterization of CoO/TUD-1 Material

The amorphous nature of the prepared catalyst was examined using XRD studies. Figure 1 depicts the wide angle XRD diffraction pattern of calcined CoO/TUD-1. The presence of a broad peak in the range of 10-40° indicates the amorphous nature of silica [38,39]. No peaks corresponding to cobalt oxide species are visible; this might be due to the fact that they were incorporated into the silica framework, or they may have been distributed homogeneously through mesoporous TUD-1 channels [29]. The mesoporosity of the catalyst, the specific surface area and volume of the pores and the characteristics that enabled bonding between the active sites and the guest molecules on the surface of the pores and across the bulk of the material were examined by Brunauer–Emmett–Teller (BET). Figure 2a illustrates the sorption isotherm of CoO/TUD-1, representing a type-IV adsorption according to the IUPAC classification, indicating the mesoporous structure of CoO/TUD-1 [40]. Further, at a relative pressure range of 0.7 to 0.9 P/Po, a large intake of nitrogen was well observed. This is due to the capillary condensation that occurs in mesoporous structure [26]. The pore sizes distributions were found to be narrow, with calculated values in the range of 6.8 nm. Based on the Barrett–Joyner–Halenda (BJH) method, the surface area was estimated to be 420 m^2/g.
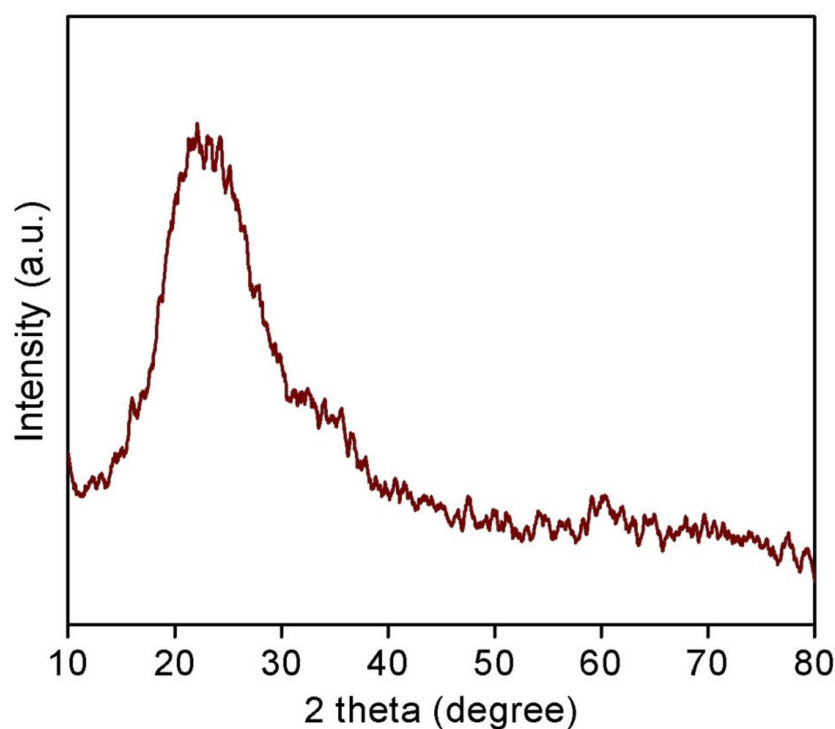

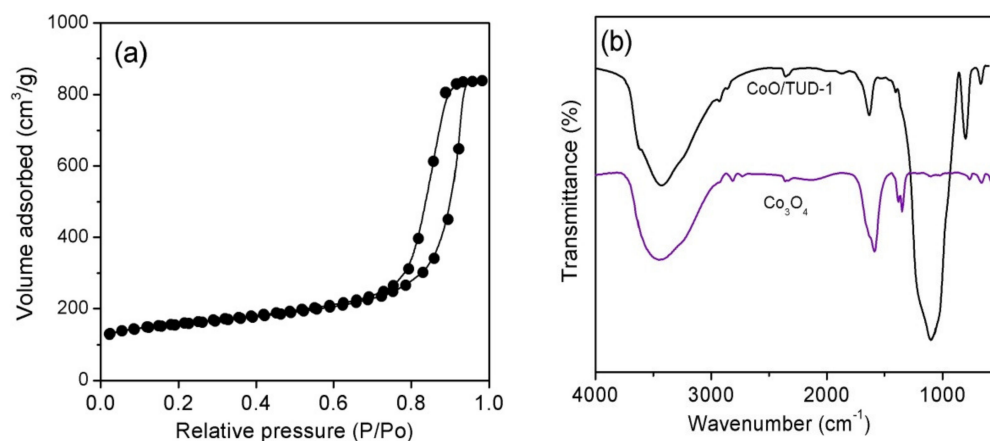
Figure 1. Wide angle powder XRD patterns of CoO/TUD-1.

Figure 2. (**a**) Nitrogen adsorption-desorption isotherm of CoO/TUD-1 and (**b**) FTIR spectrum of calcined CoO/TUD-1 and pure Co_3O_4.

The chemical functional groups present on the surface of the calcined CoO/TUD-1 and pure Co_3O_4 were studied using FT-IR, as shown in Figure 2b. The presence of a broad band around 3460 cm^{-1} was attributed to the O–H stretching vibration of the water molecules adsorbed over the catalyst's system or its surface silanol groups (Si–O–H). This was reconfirmed through the corresponding bending vibration mode formed at 1640 cm^{-1}. The asymmetrical and symmetrical stretching vibrations of the Si–O–Si bond present in the TUD-1 were confirmed through the intense vibration bands detected at 1238, 1087 and 804 cm^{-1}. Further, these bands are absent in pure Co_3O_4. The formation of an absorption band at 962 cm^{-1} was ascribed to the stretching vibration of the Si–O units bound to Co or H [29,41]. Notably, the smaller peaks noticed at 578 and 669 cm^{-1} corresponded to Co-oxygen vibrational modes.

The UV-visible DR spectra of the CoO/TUD-1 and the Co_3O_4 are illustrated in Figure 3. The peak noticed at 520 nm was assigned to the framework connected to the Co species, which is common for Co-modified mesoporous materials. Notably, compared with the Co_3O_4 absorbance bands, a broad absorbance band at a 356 nm wavelength region was detected in the CoO/TUD-1 sample. A shift in wavelength towards the lower region was associated with the non-framework octahedral coordinated Co^{3+} in the Co_3O_4 species [29]. From this observation, it was confirmed that cobalt was coordinated with silica. The bonding of Si, O and cobalt oxide in the CoO/TUD-1 catalyst is presented in Scheme 1.

To capture the morphology of the catalyst, SEM and TEM studies were performed. The SEM images, shown in Figure 4a–c, revealed the foam- or stone-like morphology of the 5 wt.% of cobalt (confirmed from Energy Dispersive X-ray Analysis (EDAX)) doped catalyst. Further, the TEM images shown in Figure 4d,e clearly depict a 3D sponge-like structure, which confirm that CoO/TUD-1 is a mesoporous material. The dark spots in the catalyst indicate the silica and cobalt species with uniform dispersion over the surface of silicon framework. This confirms the anchoring of the cobalt species over TUD-1 that facilitated the efficiency of the catalytic reaction and its stability. It is clear from the image that the presence of a 3D mesoporous structure in CoO/TUD-1 is an ideal catalytic system for many chemical reactions.

3.2. Methyl Blue Dye Degradation over CoO/TUD-1

3.2.1. About the Model

Tielens et al. proposed and confirmed the slab model of the amorphous silica (SiO$_2$) TUD-1's geometry and successfully applied the of grafting various metal and metal oxides on its surface [42–46]. The unit cell parameters of the silica's surface (a= 12.77 Å, b = 17.64 Å, c = 25.17 Å), consisted of 120 atoms ($Si_{27}O_{67}H_{26}$). In this study, the original surface of the silica featured a silanol number of 5.8 OH nm^{-2} and was partially dehydroxylated to mimic the catalyst calcination conditions [46]. The final dehydroxylated surface of the

silica model had a silanol density of 3.1 OH nm^{-2} ($Si_{27}O_{64}H_{20}$) [46]. The single cobalt atom embedded onto the silica's surface and the cobalt atom coverage in our modelled surface was around 0.4 atoms nm^{-2}. At the same coverage, the Philips catalyst achieved the highest activity [46].

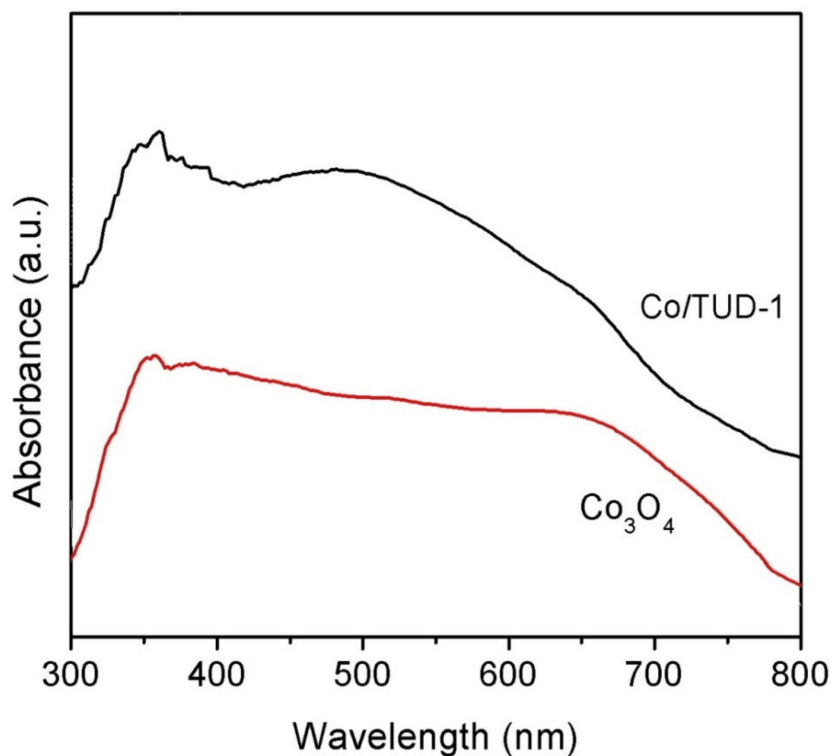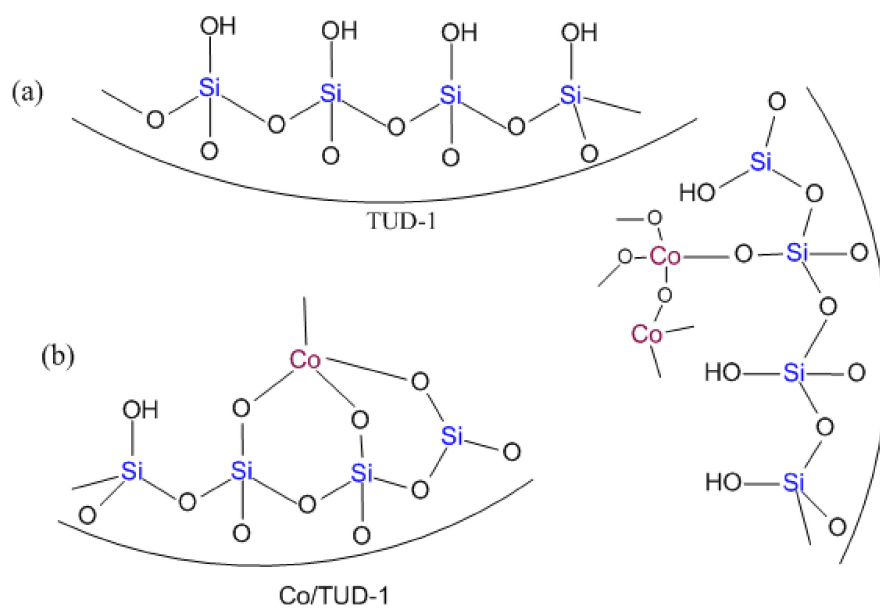**Figure 3.** UV-visible diffuse reflectance spectra of CoO/TUD-1 and pure Co_3O_4.

Scheme 1. (**a**) Proposed structure of TUD-1, (**b**) proposed structure of possible bonding in CoO/TUD-1 catalyst formation.
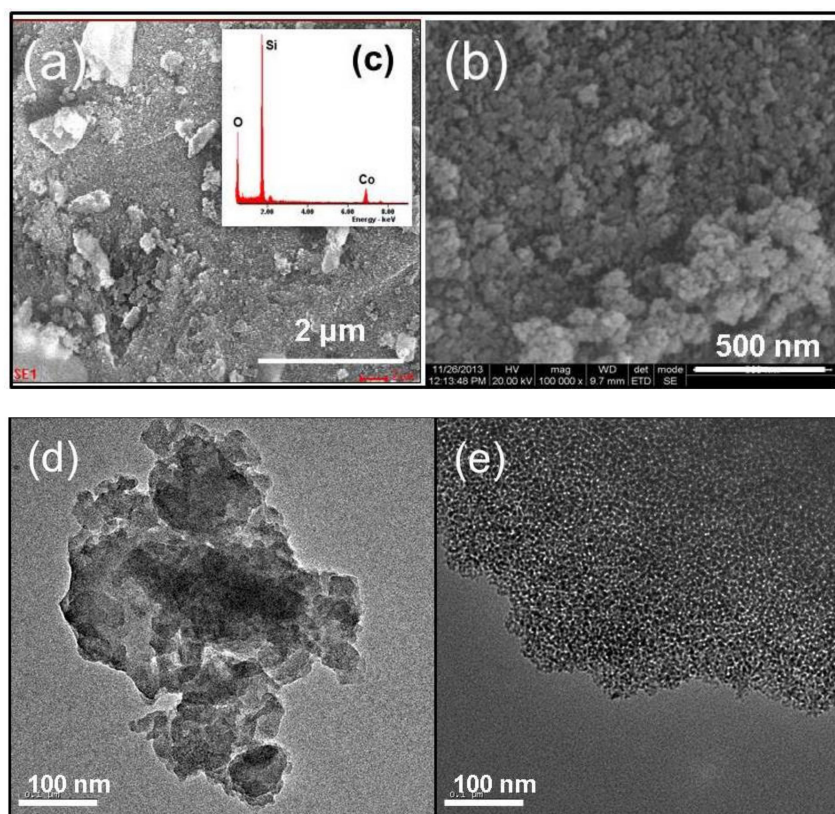
Figure 4. SEM images: (**a**–**c**) EDAX; and (**d**,**e**) TEM images of CoO/TUD-1.

3.2.2. Adsorption of Single Co Atom

DFT calculations were performed to study the most stable tetracoordinate adsorption configuration of the single Co atom on TUD-1. The single Co atom was dispersed on the amorphous SiO_2 TUD-1 surface over its oxygen (O) atoms through the dissociation of the corresponding hydrogen (H) atoms to form Co–O–Si bonds. Different kinds of tetracoordinate adsorption configurations were investigated and the corresponding calculated binding energy is shown in Figure S1. The obtained binding energies of the different coordination modes were −2.69 to −2.80 eV, indicating that all the six configurations were energetically stable. In this configuration, A was more stable than the other configurations; the most stable optimized geometry of CoO/TUD-1 (A) and the corresponding geometrical parameters are shown in Figure 5.

To understand the geometric and electronic structure of configuration A, we studied the electron density differences, Bader charge and partial density of states (PDOS). As can be seen from the electron density differences (EDD) plot in Figure 6a, there was a noticeable electron transfer from the Co atom to the am-SiO_2, and the obtained Bader charge of the Co atom (1.21 |e|) was consistent with the experimental oxidation state of cobalt (II). The electron spin density CoO/TUD-1 of 2.89 corresponded to a high spin and three unpaired electrons in cobalt with the d7 electronic configuration [47,48]. To gain a good understanding of the interaction of CoO/TUD-1, the PDOS was performed, and the results are displayed in Figure 6b. The robust contact between the Co and O of TUD-1 was further established by the formation of overlapped peaks. Furthermore, Co-3d and 2π* states of O were observed near to the Fermi level (EF), suggesting the strong interaction between the Co and O atoms.

3.2.3. Adsorption of Methylene Blue on CoO/TUD-1

We considered three different possible adsorption configurations, as shown in Figure 7. The calculated adsorption energy (E_{ad}) of the parallel configuration was −1.58 eV, and vertical configurations, such as S-top and S-down, were −1.29 eV and −1.12 eV respectively,

which indicated that methylene blue adsorbed more strongly in the parallel configuration mode and degraded more easily.
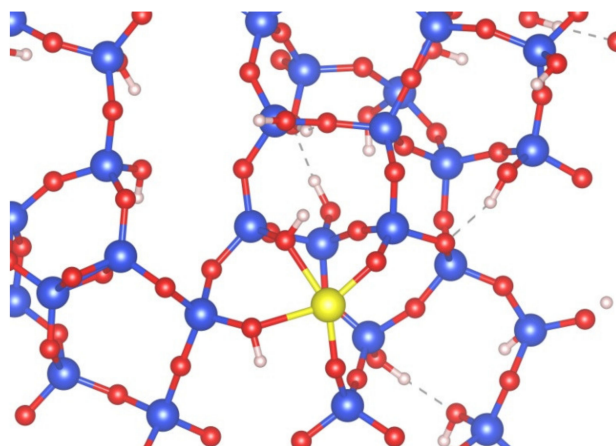

Figure 5. The optimized geometry of CoO/TUD-1. The bond lengths are given in Å. The blue, red and yellow spheres represent Si, O and Co, respectively.
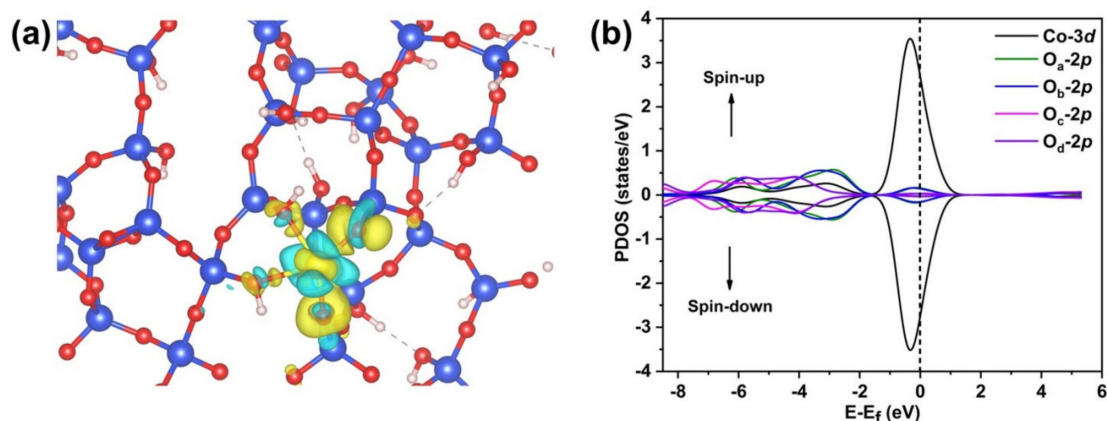

Figure 6. (**a**) Electron density differences (EDD). For the contour plots, the charge accretion areas are displayed in yellow, while the charge deduction areas are displayed in cyan. (**b**) The PDOS of Co-3d (black) and O-2p (Oa (green), Ob (blue), Oc (magenta) and Od (purple) states. The Fermi level was set to zero, as shown by the dashed line.
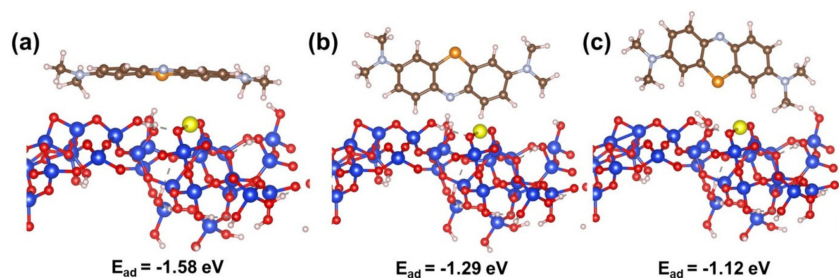

Figure 7. Three different adsorption configurations of methylene blue on TUD-1 surface: (**a**) Parallel; (**b**) vertical S-top; and (**c**) vertical S-down.

3.2.4. Degradation of Methylene Blue on CoO/TUD-1 Catalyst

Methylene blue (MB) is a cationic thiazine dye, which contains condensed rings with sulphur heteroatoms [49]. The chromophoric absorptions (λ_{max}) of the MB dye were observed at 665 nm and 291 nm in the UV-visible spectrum (Figure 8). The effect of the oxidant concentration on the reaction at different time intervals is illustrated in Figure 8b. Within a short time (below 30 min), the MB degradation began, owing to the degradation of

the MB compound with hydroxyl radicals ($°OH$), which were produced on the Co surface. As the reaction time increased, the reduction of MB also increased linearly for all the three peroxide concentrations. The calculated rate constant suggested that the increase in the H_2O_2 concentration increased the rate of reaction significantly. The observed rate constants were 0.003, 0.014 and 0.019 min^{-1}, respectively, for the different concentrations of (2.6, 6.4 and 12.8 mmol/L) H_2O_2. At 240 min, approximately 95 % of the MB molecules were degraded, which was inferred from the disappearance of the chromophore absorption intensities for 12.8 mmol/L. Hence, the addition of 12.8 mmol/L of H_2O_2 was sufficient for the stoichiometric production of hydroxyl radicals on the CoO/TUD-1 catalyst for the degradation of the MB dye. These optimum conditions were chosen for further studies.
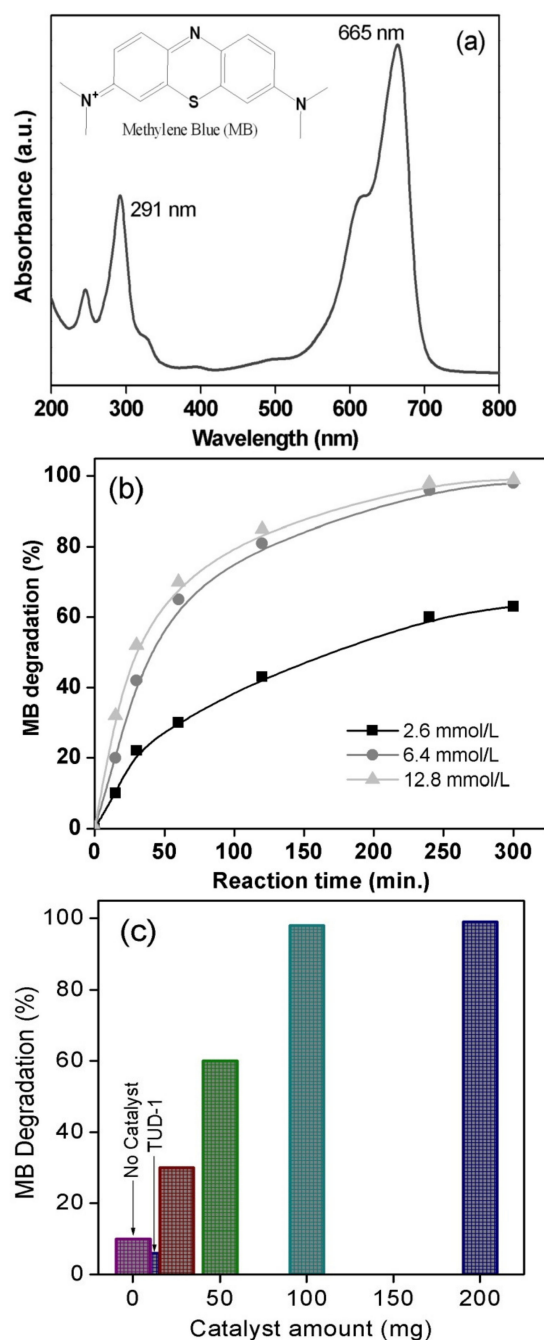

Figure 8. (**a**) UV-visible spectrum of MB. (**b**) Influence of H_2O_2 oxidant concentration on MB degradation at different time intervals. (**c**) Influence of catalyst dose on MB degradation (Reaction conditions: 100 ppm MB, 0.0–0.2 g catalyst, 2.6–12.8 mmol/L H_2O_2).

Figure 8c depicts the degradation of the MB dye in the presence of the CoO/TUD-1 catalyst with 12.8 mmol/L of H_2O_2. When the reaction proceeded, a low amount of catalyst (below 50 mg) was noticed below 60 % degradation activity. This could be explained by the fact that the addition of the catalyst could only increase the available active sites for the synergistic adsorption and catalytic degradation of MB, and thus the low amount of catalyst might have generated a lower amount of radicals. The catalytic dose of 0.1 g/L and 0.2 g/L revealed a significant increase in degradation ability (~95 %), which signified that effective radical generation was directly proportional to the available active sites for the reaction mixture. Further, a 0.1 g/L dose of catalyst was itself sufficient to achieve 95 % degradation of the MB. Hence, the optimum catalyst dose was 0.1 g/L for the degradation of 100 ppm MB solution. Interestingly, in the absence of the CoO/TUD-1 catalyst i.e., a homogeneous oxidation process, only 10 % MB degradation was achieved. This clearly confirms that the presence of the CoO/TUD-1 catalyst significantly enhanced the radical formation potential and was thus responsible for the MB degradation. This result clearly indicates the importance of the Co catalyst for the generation of hydroxyl ($°OH$) and peroxyl ($°OOH$) radicals [28,29]. Similar Fenton-type radical-generated molecular degradations are reported for CuTUD-1 and FeTUD-1 catalysts.

4. Conclusions

In summary, cobalt-loaded TUD-1 prepared by the hydrothermal method exhibited an amorphous, three-dimensional, disordered structure, with cobalt dispersed in the mesoporous channels. In the FT-IR analysis, the asymmetrical and symmetrical stretching vibrations of the Si–O–Si bond present in the TUD-1 were confirmed by the intense vibration bands detected at 1238, 1087 and 804 cm^{-1}. The resulting materials exhibited a surface area of 420 m^2/g, a pore size of 6.8 nm and an octahedrally coordinated Co^{3+} species. The DFT studies further confirmed the occurrence of electron transfers from the cobalt to the TUD-1 during the degradation reaction. Furthermore, the calculated adsorption energy clearly established the fact that the parallel absorption configuration on the Co/TUD-1 provided better adsorption and degradation of MB. The optimum time, the H_2O_2 and the catalyst amount required for the degradation were found to be 240 min, 12.8 mmol/L and 0.1 g/L, respectively. In the case of the CoO/TUD-1, dispersed, accessible Co^{2+} and Co^{3+} species were present on the TUD-1's surface; three-dimensional porous structures and MB molecular orientation near to the active sites helped to degrade 90% of the dye molecules. Thus, CoO/TUD-1 can be utilized as a promising material for the removal of organic pollutants present in wastewater.

Acronym and Abbreviations

TUD-1   Technische Universiteit Delft
DFT   Density Functional Theory
MB   methylene blue
TEOS   Tetraethyl orthosilicate
TEA   Triethanolamine
TEAOH   Tetraethyl ammonium hydroxide
VASP   Vienna ab initio simulation package
PAW   Projector augmented wave
PBE   Perdew$-$Burke$-$Ernzerhof
EDD   Electron density differences
EF   Fermi level
E_{ad} adsorption energy

References

1. Khan, S.T.; Malik, A. Engineered nanomaterials for water decontamination and purification: From lab to products. *J. Hazard. Mater.* **2019**, *363*, 295–308. [CrossRef]
2. Crini, G.; Lichtfouse, E. Advantages and disadvantages of techniques used for wastewater treatment, Environ. *Chem. Lett.* **2019**, *17*, 145–155. [CrossRef]
3. Bolisetty, S.; Peydayesh, M.; Mezzenga, R. Sustainable technologies for water purification from heavy metals: Review and analysis. *Chem. Soc. Rev.* **2019**, *48*, 463–487. [CrossRef]
4. Rafatullah, M.; Sulaiman, O.; Hashim, R.; Ahmad, A. Adsorption of methylene blue on low-cost adsorbents: A review. *J. Hazard. Mater.* **2010**, *177*, 70–80. [CrossRef] [PubMed]
5. Sangpour, P.; Hashemi, F.; Moshfegh, A.Z. Photoenhanced degradation of methylene blue on cosputtered M:TiO$_2$ (M = Au, Ag, Cu) nanocomposite systems: A comparative study. *J. Phys. Chem. C* **2010**, *114*, 13955–13961. [CrossRef]
6. Wu, Q.; Zhang, H.; Zhou, L.; Bao, C.; Zhu, H.; Zhang, Y. Synthesis and application of rGO/CoFe$_2$O4 composite for catalytic degradation of methylene blue on heterogeneous Fenton-like oxidation. *J. Taiwan Inst. Chem. Eng.* **2016**, *67*, 484–494. [CrossRef]
7. Houas, A.; Lachheb, H.; Ksibi, M.; Elaloui, E.; Guillard, C.; Herrmann, J.M. Photocatalytic degradation pathway of methylene blue in water. *Appl. Catal. B Environ.* **2001**, *31*, 145–157. [CrossRef]
8. Ong, S.A.; Toorisaka, E.; Hirata, M.; Hano, T. Biodegradation of redox dye Methylene Blue by up-flow anaerobic sludge blanket reactor. *J. Hazard. Mater.* **2005**, *124*, 88–94. [CrossRef]
9. Liu, Y.; Jin, W.; Zhao, Y.; Zhang, G.; Zhang, W. Enhanced catalytic degradation of methylene blue by A-Fe$_2$O$_3$/graphene oxide via heterogeneous photo-Fenton reactions. *Appl. Catal. B Environ.* **2017**, *206*, 642–652. [CrossRef]
10. Cheng, S.; Oatley, D.L.; Williams, P.M.; Wright, C.J. Characterisation and application of a novel positively charged nanofiltration membrane for the treatment of textile industry wastewaters. *Water Res.* **2012**, *46*, 33–42. [CrossRef]
11. Kim, S.; Yu, M.; Yoon, Y. Fouling and Retention Mechanisms of Selected Cationic and Anionic Dyes in a Ti$_3$C$_2$Tx MXene-Ultrafiltration Hybrid System. *ACS Appl. Mater. Interfaces* **2020**, *12*, 16557–16565. [CrossRef]
12. Mudliar, R.; Umare, S.S.; Ramteke, D.S.; Wate, S.R. Energy efficient—Advanced oxidation process for treatment of cyanide containing automobile industry wastewater. *J. Hazard. Mater.* **2009**, *164*, 1474–1479. [CrossRef]
13. Mandal, T.; Maity, S.; Dasgupta, D.; Datta, S. Advanced oxidation process and biotreatment: Their roles in combined industrial wastewater treatment. *Desalination* **2010**, *250*, 87–94. [CrossRef]
14. Nidheesh, P.V.; Gandhimathi, R.; Ramesh, S.T. Degradation of dyes from aqueous solution by Fenton processes: A review. *Environ. Sci. Pollut. Res.* **2013**, *20*, 2099–2132. [CrossRef]
15. Wang, Q.; Tian, S.; Ning, P. Ferrocene-catalyzed heterogeneous fenton-like degradation of methylene blue: Influence of initial solution pH. *Ind. Eng. Chem. Res.* **2014**, *53*, 6334–6340. [CrossRef]
16. Jia, Z.; Kang, J.; Zhang, W.C.; Wang, W.M.; Yang, C.; Sun, H.; Habibi, D.; Zhang, L.C. Surface aging behaviour of Fe-based amorphous alloys as catalysts during heterogeneous photo Fenton-like process for water treatment. *Appl. Catal. B Environ.* **2017**, *204*, 537–547. [CrossRef]
17. Wang, Q.; Chen, M.; Lin, P.; Cui, Z.; Chu, C.; Shen, B. Investigation of FePC amorphous alloys with self-renewing behaviour for highly efficient decolorization of methylene blue. *J. Mater. Chem. A* **2018**, *6*, 10686–10699. [CrossRef]
18. Liang, S.X.; Wang, X.; Zhang, W.; Liu, Y.; Wang, W.; Zhang, L.C. Selective laser melting manufactured porous Fe-based metallic glass matrix composite with remarkable catalytic activity and reusability. *Appl. Mater. Today* **2020**, *19*, 100543. [CrossRef]
19. Liang, S.X.; Jia, Z.; Liu, Y.; Zhang, W.; Wang, W.; Lu, J.; Zhang, L.C. Metallic Glasses: Compelling Rejuvenated Catalytic Performance in Metallic Glasses. *Adv. Mater.* **2018**, *30*, 1–11. [CrossRef]
20. Kirchon, A.; Zhang, P.; Li, J.; Joseph, E.A.; Chen, W.; Zhou, H.C. Effect of Isomorphic Metal Substitution on the Fenton and Photo-Fenton Degradation of Methylene Blue Using Fe-Based Metal-Organic Frameworks. *ACS Appl. Mater. Interfaces* **2020**, *12*, 9292–9299. [CrossRef] [PubMed]

21. Dou, R.; Cheng, H.; Ma, J.; Qin, Y.; Kong, Y.; Komarneni, S. Catalytic degradation of methylene blue through activation of bisulfite with CoO nanoparticles. *Sep. Purif. Technol.* **2020**, *239*, 116561. [CrossRef]

22. Bibi, I.; Nazar, N.; Iqbal, M.; Kamal, S.; Nawaz, H.; Nouren, S. Green and eco-friendly synthesis of cobalt-oxide nanoparticle: Characterization and photo-catalytic activity. *Adv. Powder Technol.* **2017**, *28*, 2035–2043. [CrossRef]

23. Hu, P.; Long, M.; Environ, A.C.B. Cobalt-catalyzed sulfate radical-based advanced oxidation: A review on heterogeneous catalysts and applications. *Appl. Catal. B Environ.* **2016**, *181*, 103–117. [CrossRef]

24. Shukla, P.R.; Wang, S.; Sun, H.; Ang, H.M.; Tadé, M. Activated carbon supported cobalt catalysts for advanced oxidation of organic contaminants in aqueous solution. *Appl. Catal. B Environ.* **2010**, *100*, 529–534. [CrossRef]

25. Stoyanova, M.; Slavova, I.; Christoskova, S.; Ivanova, V. Catalytic performance of supported nanosized cobalt and iron–cobalt mixed oxides on MgO in oxidative degradation of Acid Orange 7 azo dye with peroxymonosulfate. *Appl. Catal. A Gen.* **2014**, *476*, 121–132. [CrossRef]

26. Hamdy, M.S.; Ramanathan, A.; Maschmeyer, T. Co-TUD-1: A Ketone-Selective Catalyst for Cyclohexane Oxidation. *Chem. Eur. J.* **2006**, 1782–1789. [CrossRef]

27. Hamdy, M.S.; Mul, G.; Wei, W.; Anand, R.; Hanefeld, U. Fe, Co and Cu-incorporated TUD-1: Synthesis, characterization and catalytic performance in N_2O decomposition and cyclohexane oxidation. *Catal. Today* **2005**, *110*, 264–271. [CrossRef]

28. Pachamuthu, M.P.; Karthikeyan, S.; Maheswari, R.; Lee, A.F.; Ramanathan, A. Fenton-like degradation of Bisphenol A catalyzed by mesoporous Cu/TUD-1. *Appl. Surf. Sci.* **2017**, *393*, 67–73. [CrossRef]

29. Pachamuthu, M.P.; Rajalakshmi, R. RSC Advances Direct glycol assisted synthesis of an amorphous mesoporous silicate with framework incorporated Co^{2+}: Characterization and catalytic application in ethylbenzene oxidation. *RSC Adv.* **2014**, *4*, 29909–29916. [CrossRef]

30. Kresse, G.; Furthmüller, J. Efficiency of ab-initio total energy calculations for metals and semiconductors using a plane-wave basis set. *Comput. Mater. Sci.* **1996**, *6*, 15–50. [CrossRef]

31. Kresse, G.; Hafner, J. Ab initio molecular dynamics for liquid metals. *Phys. Rev. B* **1993**, *47*, 558–561. [CrossRef] [PubMed]

32. Kresse, G.; Hafner, J. Ab initio molecular-dynamics simulation of the liquid-metal–amorphous-semiconductor transition in germanium. *Phys. Rev. B* **1994**, *49*, 14251–14269. [CrossRef]

33. Blöchl, P.E. Projector augmented-wave method. *Phys. Rev. B* **1994**, *50*, 17953–17979. [CrossRef]

34. Perdew, J.P.; Burke, K.; Ernzerhof, M. Generalized Gradient Approximation Made Simple. *Phys. Rev. Lett.* **1996**, *77*, 3865–3868. [CrossRef] [PubMed]

35. Grimme, S. Semiempirical GGA-type density functional constructed with a long-range dispersion correction. *J. Comput. Chem.* **2006**, *27*, 1787–1799. [CrossRef]

36. Tang, W.; Sanville, E.; Henkelman, G. A grid-based Bader analysis algorithm without lattice bias. *J. Phys. Condens. Matter.* **2009**, *21*, 1–7. [CrossRef] [PubMed]

37. Yu, M.; Trinkle, D.R. Accurate and efficient algorithm for Bader charge integration. *J. Chem. Phys.* **2011**, *134*, 1–8. [CrossRef] [PubMed]

38. Liang, S.X.; Jia, Z.; Zhang, W.C.; Li, X.F.; Wang, W.M.; Lin, H.C.; Zhang, L.C. Ultrafast activation efficiency of three peroxides by Fe78Si9B13 metallic glass under photo-enhanced catalytic oxidation: A comparative study. *Appl. Catal. B Environ.* **2018**, *221*, 108–118. [CrossRef]

39. Miao, F.; Wang, Q.; Di, S.; Yun, L.; Zhou, J.; Shen, B. Enhanced dye degradation capability and reusability of Fe-based amorphous ribbons by surface activation. *J Material Sci. Tech.* **2020**, *53*, 163–173. [CrossRef]

40. Anand, R.; Hamdy, M.S.; Hanefeld, U.; Maschmeyer, T. Liquid-phase oxidation of cyclohexane over Co-TUD-1. *Catal. Lett.* **2006**, *95*, 113–117. [CrossRef]

41. Pachamuthu, M.P.; Shanthi, K.; Luque, R.; Ramanathan, A. SnTUD-1: A Solid Acid Catalyst for Three Component coupling reactions at room temperature. *Green Chem.* **2013**, *15*, 2158–2166. [CrossRef]

42. Islam, M.M.; Costa, D.; Calatayud, M.; Tielens, F. Characterization of Supported Vanadium Oxide Species on Silica: A Periodic DFT Investigation. *J. Phys. Chem. C* **2009**, *113*, 10740–10746. [CrossRef]

43. Wojtaszek, A.; Sobczak, I.; Ziolek, M.; Tielens, F. Gold Grafted to Mesoporous Silica Surfaces, a Molecular Picture. *J. Phys. Chem. C* **2009**, *113*, 13855–13859. [CrossRef]

44. Tranca, D.C.; Wojtaszek-Gurdak, A.; Ziolek, M.; Tielens, F. Supported and inserted monomeric niobium oxide species on/in silica: A molecular picture. *Phys. Chem. Chem. Phys.* **2015**, *17*, 22402–22411. [CrossRef] [PubMed]

45. Siodla, T.; Sobczak, I.; Ziolek, M.; Tielens, F. Theoretical and experimental insight into zinc loading on mesoporous silica. *Microporous Mesoporous Mater.* **2018**, *256*, 199–205. [CrossRef]

46. Handzlik, J.; Grybos, R.; Tielens, F. Structure of Monomeric Chromium(VI) Oxide Species Supported on Silica: Periodic and Cluster DFT Studies. *J. Phys. Chem. C* **2013**, *117*, 8138–8149. [CrossRef]

47. Vankimmenade, E.; Kuiper, A.; Tamminga, Y.; Thune, P.; Niemantsverdriet, J. A surface science model for the Phillips ethylene polymerization catalyst: Thermal activation and polymerization activity. *J. Catal.* **2004**, *223*, 134–141. [CrossRef]

48. Hu, B.; Schweitzer, N.M.; Das, U.; Kim, H.; Niklas, J.; Poluektov, O.; Curtiss, L.A.; Stair, P.C.; Miller, J.T.; Hock, A.S.; et al. Selective propane dehydrogenation with single-site CoII on SiO2 by a non-redox mechanism. *J. Catal.* **2015**, *322*, 24–37. [CrossRef]

49. Vandarkuzhali, S.A.A.; Karthikeyan, S.; Viswanathan, B.; Pachamuthu, M.P. Arachis hypogaea derived activated carbon/Pt catalyst: Reduction of organic dyes. *Surf. Interfaces* **2018**, *13*, 101–111. [CrossRef]